

Low-Latency Broadband Analog Aggregation for Federated Edge Learning

Guangxu Zhu, Yong Wang and Kaibin Huang

Abstract

The popularity of mobile devices and densification of telecommunication networks result in the availability of enormous data and computational resources distributed at the network edge. To leverage the data and resources, a new machine-learning paradigm, called edge learning, has emerged where learning algorithms are deployed at the edge for providing fast and intelligent services to mobile users. While computing speeds are advancing rapidly, the communication latency is becoming the bottleneck of fast edge learning. To address this issue, this work is focused on designing a low-latency multi-access scheme for edge learning. To this end, we consider a popular framework, *federated edge learning* (FEEL), where edge-server and on-device learning are synchronized to train a model without violating user-data privacy. It is proposed that model updates simultaneously transmitted by devices over broadband channels should be analog aggregated (averaged) “over-the-air” by exploiting the inherent waveform-superposition property of a multi-access channel. Thereby, “interference” is harnessed to provide fast implementation of the model aggregation, a key FEEL operation. This results in dramatical latency reduction compared with the traditional orthogonal access (i.e., OFDMA). In this work, the performance of FEEL is characterized targeting a single-cell random network. First, due to power alignment between devices as required for aggregation, a fundamental reliability-and-truncation tradeoff is shown to exist between the update-reliability (as measured by received SNR) and the expected update-truncation ratio. This motivates the design of an opportunistic scheduling scheme for FEEL that selects device within a distance threshold. This scheme is shown using real datasets to yield close-to-optimal learning performance in the presence of high mobility. Second, both the multi-access latency of the proposed analog aggregation and the traditional OFDMA scheme are analyzed. Their ratio, which quantifies the latency reduction of the former, is proved to scale almost linearly with device population. In addition, we investigate the extensions of broadband analog aggregation to include scrambling for safety against adversary attacks and beamforming for alleviating the performance bottleneck due to cell-edge devices.

I. INTRODUCTION

The traffic in mobile Internet is growing at a breath-taking rate due to the extreme popularity of mobile devices (e.g., smartphones and sensors). Analysis shows that there will be 80 billions of devices connected to Internet by 2025, resulting in a tenfold traffic growth compared with 2016 [1]. The availability of enormous mobile data and recent breakthroughs in *artificial intelligence* (AI) motivate researchers to develop AI technologies at the network edge. Such technologies are collectively called edge AI and represent a latest trend in machine learning, i.e., *edge learning*, that concerns training of edge-AI models

G. Zhu, Y. Wong and K. Huang are with the Dept. of Electrical and Electronic Engineering at The University of Hong Kong, Hong Kong (Email: gxzhu@eee.hku.hk, wangyong@eee.hku.hk, huangkb@eee.hku.hk). Corresponding author: K. Huang.

using the emerging *mobile edge computing* (MEC) platform [2]–[4]. The migration of learning from central clouds towards the edge allows edge servers to have fast access to big data generated by edge devices in real time for fast training of AI models. In return, downloading the trained models to the devices provision them intelligence to respond to real-time events. Targeting fast intelligence acquisition, fast data processing and fast data acquisition are two key features to be pursued in edge learning. While computing speeds are growing rapidly due to the emergence of powerful AI chips, e.g., *graphics processing units* (GPUs) and *tensor processing units* (TPUs), wireless data acquisition suffers from scarcity of radio resources and hostility of wireless channels, resulting in a communication bottleneck for fast edge learning [5], [6].

Motivated by this, a new edge learning paradigm, called *federated edge learning* (FEEL), is developed recently, which features distributed learning at edge devices and local-update averaging at an edge server [6], [7]. In contrast to the conventional centralized model training, FEEL is more communication-efficient as no raw data but only the locally computed updates on the AI model are uploaded to the server. Along with the reduced communication cost, it provides better user-privacy protection as no personal data gets exposed over-the-air during the distributed learning federation. Nevertheless, the updates uploading in FEEL can be still bandwidth-consuming as an AI model usually comprises millions to billions of parameters. Particularly, the high-dimensional updates from dense edge devices via orthogonal multiple access may incur unacceptable latency that scales with the device population. The scaling-up latency is arguably an artifact of the classic approach of “transmit-then-compute” as the edge server is only interested in the mean value of distributed updates instead of their individual values. Therefore, the recently developed multiple access scheme called “*over-the-air*” *computation* (AirComp) is particularly appealing in the scenario as it integrates transmission and computation and allows “one-shot” data aggregation by exploiting the waveform-superposition property of a multi-access channel (MAC). Theoretically, AirComp, that harnesses interference from concurrent transmission for functional computation, can dramatically reduce the data aggregation latency by a factor equal to the number of devices. The promising theoretical gain inspires us to develop in the current work a framework of low-latency update-aggregation scheme exploiting AirComp for FEEL.

A. Federated Edge Learning

As mentioned, FEEL is a recently developed learning paradigm featuring high communication efficiency and user-privacy protection. Specifically, a typical federated-learning algorithm alternates between two phases, as shown in Fig. 1. One is to aggregate distributed updates over a MAC and apply their average to update the AI-model at the edge server. The other is to broadcast the model under training to allow edge devices to continuously refine their individual versions of the model. The iteration continues until the global model converges and each iteration is called a *communication round*. The updates locally computed at edge devices can be either the model coefficients [6] or gradient vectors [7], giving rise two implementation approaches, i.e., *model-averaging* and *gradient-averaging*.

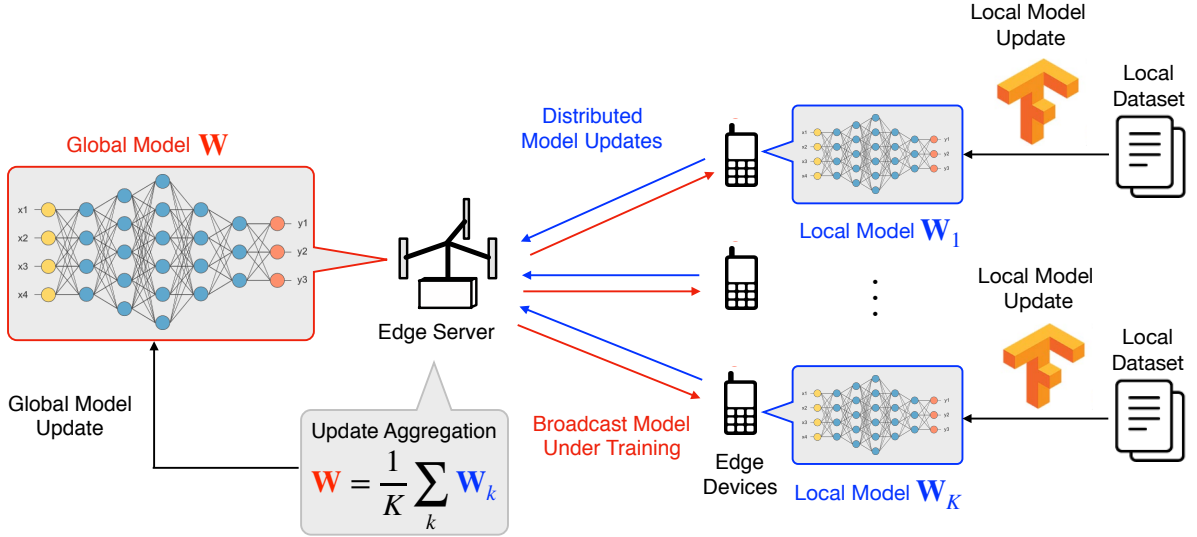


Figure 1. Federated edge learning from wirelessly distributed data.

In view of high dimensionality in updates, a key research issue that is particularly hot recently is to reduce the overhead in update uploading to further accelerate the model training process. Along this vein, an increasing amount of research effort has been dedicated to developing efficient update-aggregation solutions [8]–[13]. Among them, a branch of research focus on addressing the *straggler effect* in synchronous update averaging (namely, the slowest device dominates the overall updating latency due to synchronization). Particularly, a partial model averaging scheme is proposed in [8], where, instead of averaging full number of updates from all devices, only a portion of fast responding devices' updates will be used to update the global model. Later, the design was further enhanced by applying coding techniques to the updates such that the desired full update-averaging can be still computed with only a portion of coded updates [9]. Another series of research focuses on developing lazily updating algorithm that schedules only those devices with significant updates to save the updating bandwidth. Depending on whether the model or gradient update is adopted, the significance of an update is either measured by the *model variance* which indicates the divergence of a particular local model to the average value across all local models [10], or *gradient divergence* that reflects the level of change on the current gradient update w.r.t. the previous one [11]. Another approach for reducing communication overhead is to compress gradient vectors by exploiting its inherent sparsity: most of the gradient elements are insignificant and thus can be truncated without harming the model accuracy [12], [13].

The above prior work all focus on developing generic communication-efficient updating solution by cutting unnecessary/insignificant update information where the unique property of wireless channel is unexplored. To achieve further reduction in communication overhead, an integrated communication and learning solution is essential but remains a largely uncharted area. The proposed AirComp based update-aggregation solution in the current work represents the initial but significant step towards the ongoing paradigm shift advocating communication and computation integration.

B. Over-the-Air Computation

The idea of AirComp can be traced back to the pioneering work studying functional computation in sensor networks [14]. The design relies on structured codes (i.e., lattice codes) to cope with channel distortion introduced by the MAC. The significance of the work lies in its counter-intuitive finding that “interference” can be harnessed to help computing. It was subsequently discovered in [15] that simple analog transmission without coding but with channel pre-equalization can achieve the minimum distortion if the data sources are independent and identically distributed (i.i.d.) Gaussian. Nevertheless, coding can be still useful for other settings if the sources follow more complex distributions such as bivariate Gaussian [16] and correlated Gaussian [17]. The satisfactory performance and simplicity of analog AirComp has led to an active area focusing on robustness design and performance analysis [18]–[21]. In particular, techniques for distributed power control and robust AirComp against channel estimation errors are respectively proposed in [18] and [19]. Theoretical analysis on the AirComp outage performance under a distortion constraint and the computation rate, defined as the number of functional values computed per time slot, were provided in [20] and [21], respectively. Another vein of research focuses on transforming AirComp from theory into practice by prototyping [22] and addressing the practical issue of transmission synchronization over sensors [23], [24]. In [23], the authors proposed to modulate the data into transmit power to relax the synchronization requirement. As a result, only coarse block-synchronization is required for realizing AirComp. An alternative scheme, called *AirShare*, is developed in [24] which broadcasts a shared clock to all devices so as to enforce synchronization.

Going beyond scalar-valued function computation, latest trend in the area also explores MIMO techniques to enable vector-valued function computation [25]–[27], referred as MIMO AirComp. In particular, a comprehensive framework for MIMO AirComp that consists of beamforming optimization and a matching limited channel feedback design is proposed in [25]. The framework was then subsequently extended to wirelessly-powered AirComp system [26], where the beamformer was jointly optimized with the wireless power control to further reduce the AirComp distortion, and massive MIMO AirComp system [27], where a reduced-dimension two-tier beamformer design was developed by exploiting the antenna correlation and clustered channel structure to reduce the signal processing complexity. It is also worth mentioning that, while AirComp is mostly deployed in computation-centric sensor networks as discussed above, the AirComp operation has been also leveraged in rate-maximization cellular systems such as two-way relaying [28] and MIMO lattice decoding [29].

The prior work described above focuses on AirComp in narrow-band systems. The abundant spectral degrees-of-freedom (DoF) provided by the broadband system can be also exploited for high-dimensional vector-valued function computation, e.g., update-aggregation in FEEL. Nevertheless, to the best of the authors knowledge, broadband AirComp has not been reported in the existing literature. The underlying reason is that the conventional broadband solution, i.e., the orthogonal frequency division multiplexing

(OFDM) architecture, and the power control policy are designed for *digital* communication aiming at *rate maximization*, which cannot be directly applied for *analog* AirComp with a distinct objective of *computation-error minimization*. Therefore a new broadband AirComp solution is in demand.

C. Contribution and Organization

In this paper, we consider an single-cell edge learning system consisting of a single edge server and multiple edge devices. A shared model is trained at the edge server using the distributed data across edge devices. To preserve user privacy, the FEEL framework is employed where locally computed model-updates are uploaded via a shared MAC for global model updating. To break the mentioned communication latency bottleneck due to the high-dimensional update uploading, a low-latency analog update aggregation framework exploiting AirComp is developed, where the unique design tradeoffs resulting from the framework are identified. Practical solutions providing flexible control on the said tradeoffs are proposed. The performance gain of the proposed analog aggregation over the traditional orthogonal access is quantified.

We remark that, upon the completion of the paper, we are aware of a piece of parallel ongoing work [30] that also explores the analog AirComp for low-latency FEEL but with different focuses. In particular, the work [30] focuses on source coding that exploits the superposition property of a MAC and the sparsity of updates for reduced-dimension analog transmission. In contrast, we focus on power control to align the receive power from different edge devices for direct model-update aggregation over-the-air.

The main contributions of the work are elaborated as follows.

- **Broadband Analog Update Aggregation Solution.** To enforce the channel compensation so as to yield the desired aggregated model over-the-air. A truncated channel inversion power control policy is proposed, where the cutoff threshold need be selected for computation error minimization. Particularly, an unique tradeoff between the receive *signal-to-the-noise ratio* (SNR) and the *truncated ratio* of the transmitted update controlled by the cutoff threshold is identified. The optimal threshold optimizing the said tradeoff is in sharp contrast to the conventional design targeting rate maximization.
- **Opportunistic User Scheduling for High-Mobility Networks.** Given the truncated channel inversion policy, it is shown that the receive SNR of the aggregated update is limited by the furthest device due to the power alignment for aggregation among the participating devices. To avoid heavy penalty in receive SNR, a simple opportunistic scheduling scheme that schedules only the cell-interior devices within a pre-specified inner range is investigated. Essentially, the scheme trades the amount of exploited data in each communication round for a higher receive SNR. The said tradeoff controlled by the inner range parameter is analytically quantified targeting a random network with uniform device distribution. The scheme outperforms the naive scheme that schedules all users by a considerable gap when the devices are highly mobile. This is because the scheduled devices vary rapidly over time and thus ensures the data diversity exploited during the training, which makes the learning performance *noise-limited*.

- **Alternating User Scheduling for Low-Mobility Networks.** Targeting the low-mobility scenario, the opportunistic scheduling may lead to a poor learning performance due to the lack of diversity in the data exploited. In other words, the learning performance is more *data-limited* in this scenario. To tackle the issue, an alternating scheduling scheme that alternates between the opportunistic scheduling and the all-inclusive scheme is proposed. It is shown via experiment that the alternating scheme outperforms both the component schemes in low-mobility scenario. The underlying reason is that alternating can achieve a better tradeoff between the receive SNRs of the updates and the data diversity exploited for computing the updates.
- **Latency Gain Analysis for the Proposed Analog Aggregation.** The latency performance of the proposed analog aggregation is characterized and compared with that of the conventional digital aggregation scheme which employs OFDMA together with adaptive modulation that maximizes the uploading rate under a target *bit error rate* (BER). The latency gain defined as the ratio between the latency of the two schemes is derived in closed-form as a function of several key system parameters, including the user population, maximum device distance, transmit power and the BER requirement. The most important take-home insight is that the latency gain shows an approximately linear scaling with the user population, justifying the low-latency property of the proposed analog aggregation.

Organization: The remainder of the paper is organized as follows. Section II introduces the system and channel models. Section III presents the proposed broadband analog aggregation for FEEL where the design problem of user scheduling is identified. An opportunistic scheduling scheme is presented in Section IV and the tradeoff controlled by the design parameter is quantified therein. The latency performance of the proposed analog aggregation is analytically compared with the digital counterpart in Section V. Section VI shows the experimental results. Further discussion on possible extensions is provided in Section VII, followed by concluding remarks in Section VIII.

II. SYSTEM MODEL

A. Federated Edge Learning System

We consider an edge learning system comprising a single edge server and K edge devices as shown in Fig. 1. A shared AI model (e.g., a classifier), denoted by \mathbf{w} , is trained collaboratively across the edge devices each collects a fraction of labelled training data via the interaction with its own user. To facilitate the learning, the loss function measuring the trained model error is defined as follows.

Let \mathcal{D}_k denote the local dataset collected in the k -th edge devices. The *local loss function* of the model vector \mathbf{w} on \mathcal{D}_k is given by

$$\text{(Local loss function)} \quad F_k(\mathbf{w}) = \frac{1}{|\mathcal{D}_k|} \sum_{(\mathbf{x}_j, y_j) \in \mathcal{D}_k} f(\mathbf{w}, \mathbf{x}_j, y_j), \quad (1)$$

where $f(\mathbf{w}, \mathbf{x}_j, y_j)$ is the sample-wise loss function capturing the prediction error of the model \mathbf{w} on the training sample \mathbf{x}_j w.r.t. its ground-true label y_j .

For convenience, we write $f(\mathbf{w}, \mathbf{x}_j, y_j)$ as $f_j(\mathbf{w})$ in short and assume $|\mathcal{D}_k| \equiv D$, for all k . Then, the *global loss function* on all the distributed datasets can be written as

$$\text{(Global loss function)} \quad F(\mathbf{w}) = \frac{\sum_{j \in \cup_k \mathcal{D}_k} f_j(\mathbf{w})}{|\cup_k \mathcal{D}_k|} = \frac{1}{K} \sum_{k=1}^K F_k(\mathbf{w}). \quad (2)$$

The learning process is thus to minimize the global loss function $F(\mathbf{w})$, namely,

$$\mathbf{w}^* = \arg \min F(\mathbf{w}). \quad (3)$$

However, due to the distributed data setting, $F(\mathbf{w})$ cannot be directly computed without sharing data among distributed devices. To tackle the issue, the FEEL framework is employed to solve the problem in (3) in a distributed manner. We focus on model-averaging implementation in the subsequent presentation while the same principle also applies for gradient-averaging.

In FEEL, at each communication round, the edge server broadcasts the current model under training $\mathbf{w}[n]$ to all edge devices, where n is the index of the communication round. Starting from $\mathbf{w}[n]$, each device updates its own model by running τ -step ($\tau \geq 1$) *stochastic gradient descent* (SGD) to minimize the loss function defined in (1). Mathematically, for device k , a single-step SGD updates the local model \mathbf{w}_k via

$$\text{(Local model updating)} \quad \mathbf{w}_k[n+1] = \mathbf{w}[n] - \eta \nabla F_k(\mathbf{w}[n]), \quad (4)$$

where η is the step size and ∇ represents the gradient operator. Likewise, a τ -step SGD repeats the updating rule in (4) for τ times.

Then the local model-updates are sent to edge server for model-averaging to update the global model \mathbf{w} , and it follows that

$$\text{(Global model updating)} \quad \mathbf{w}[n+1] = \frac{1}{K} \sum_{k=1}^K \mathbf{w}_k[n+1]. \quad (5)$$

The learning process involves the iteration between (4) and (5) until the model convergence.

As observed in (5), it is only the aggregated model, i.e.,

$$\text{(Model aggregation)} \quad \mathbf{y} = \sum_{k=1}^K \mathbf{w}_k, \quad (6)$$

instead of individual model-updates $\{\mathbf{w}_k\}$, needed at the edge server for model averaging. This motivates the low-latency analog aggregation scheme exploiting AirComp as presented in Section III.

B. Wireless Fading Channel and Wide-Band Transmission

The uploading of model-updates from edge devices to the server is through a shared wide-band channel. To combat the frequency selective fading and avoid the inter-symbol interference, OFDM architecture

is implemented to divide the whole bandwidth B to M sub-channels. To exploit AirComp for low-latency model aggregation, model-updates are amplitude-modulated for analog transmission. Also, each sub-channel is dedicated for one model-coefficient transmission.

During the model updating phase, all devices transmit simultaneously over the whole available bandwidth. Let $\mathbf{w}_k = [w_{k,1}, w_{k,2}, \dots, w_{k,p}]$ denote the local model-update from the k -th device, where p denotes the dimension of a model-update. At each communication round, the model-updating duration consists of $T_s = \frac{p}{M}$ OFDM symbols. In particular, the i -th aggregated model coefficient, denoted by y_i , with $i = (t-1)M + m$, received in the m -th sub-carrier at the t -th OFDM symbol, is given by

$$y_i = \sum_{k=1}^K r_k^{-\frac{\alpha}{2}} h_k^{(m)}[t] f_k^{(m)}[t] w_{k,i} + z^{(m)}[t], \quad \forall i \quad (7)$$

where $r_k^{-\frac{\alpha}{2}}$ captures the path-loss of the link between device k and the edge server, with r_k denoting the distance between them and α representing the path-loss exponent; the small-scale fading of the channel is captured by $h_k^{(m)}[t]$ which follows Rayleigh fading and is *identically and independently distributed* (i.i.d.) over the indexes of k, m, t , yielding $h_k^{(m)}[t] \sim \mathcal{CN}(0, 1)$. $f_k^{(m)}[t]$ is the associated power adaptation on the transmitted updates to be designed in the sequel. Last, $z^{(m)}[t]$ models the i.i.d. *additive white Gaussian noise* (AWGN) following $\mathcal{CN}(0, 1)$. For ease of notation, we will skip the frequency and/or time indexes, i.e., m and/or t , in the subsequent presentation, whenever no confusion is incurred. Also for ease of exposition, the uploaded model coefficients are assumed to be normalized to have unit variance, i.e., $\mathbf{E}(\mathbf{w}_k \mathbf{w}_k^H) = \mathbf{I}$, where the normalization factor for each model dimension is uniform for all devices and can be inverted at the edge server.

To implement the AirComp-based model aggregation, the power adaptation factor f_k needs to be designed according to the channel coefficient h_k to ensure the desired aggregation of the model-updates at the edge server. Throughout the paper, we consider the following average power constraint on each device k , which concerns the long-term transmit power consumption.

$$\mathbf{E} \left[\sum_{m=1}^M |f_k^{(m)}(h_k^{(m)})|^2 \right] \leq P_0, \quad \forall k, \quad (8)$$

where the the expectation is taken over the random channel coefficients.

Since channel coefficients are i.i.d. over the frequency index m , the above power constraint reduces to

$$\text{(Power constraint)} \quad \mathbf{E} \left[|f_k^{(m)}(h_k^{(m)})|^2 \right] \leq \frac{P_0}{M}, \quad \forall k. \quad (9)$$

A power control policy targeting AirComp of (6) is developed under the above constraint in the sequel.

C. Network Topology

To facilitate the subsequent performance analysis, we consider a single-cell random network where the edge devices are i.i.d. distributed over a circular cell centred at the edge server with a cell-radius R . Thus

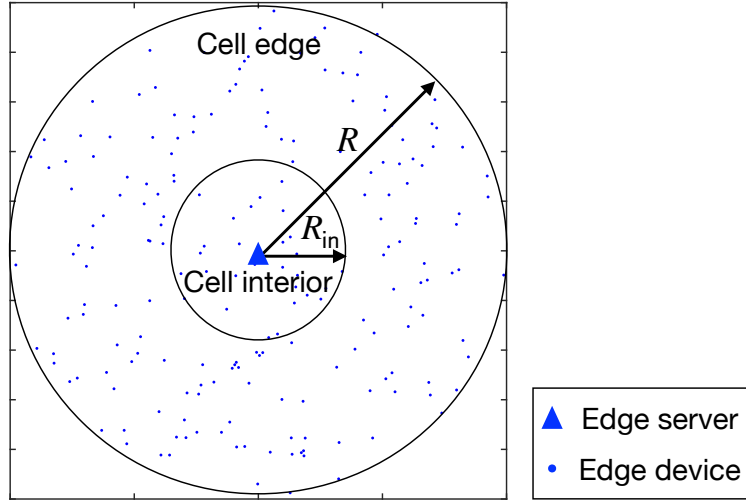


Figure 2. A single cell edge learning system with uniform distributed edge devices.

the probability density function (PDF) of the distance r_k is given by

$$f_{r_k}(r) = \frac{2r}{R^2}, \quad 0 \leq r \leq R. \quad (10)$$

Fig. 2 gives an illustrative example of the proposed uniform distributions. As will be referred to in Section IV, the whole cell will be divided into two non-overlapping parts according to the distance to the cell centre. In particular, we will refer the area within a range of a pre-specified R_{in} as the *cell-interior* while the area out of the range as *cell-edge*.

III. BROADBAND ANALOG AGGREGATION

The detailed design of analog model aggregation is presented in the current section targeting broadband system with OFDM implementation. As mentioned, AirComp is enabled by the waveform-superposition property of a MAC. Therefore, to attain the desired model aggregation over the air, AirComp requires the application of *analog amplitude modulation* to model-updates and power control for *channel-compensation* at the transmitter (see Fig. 3). Particularly, how well the channel can be compensated directly determines the quality of the aggregated update and thus governs the ultimate learning performance. Therefore, the power control policy is the core design in the framework of analog aggregation.

A. Proposed Scheme

Assuming perfect CSI at the edge devices, a naive approach to compensate the channel is to set the power adaptation factor inversely proportional to the channel coefficient, i.e., $f_k \propto \frac{1}{h_k}$. However, given a power constraint, the complete channel inversion scheme may lead to extremely low SNR, since much of the transmit power will be wasted on the compensation of deep fading. Particularly, it is known that the scheme is not feasible for Rayleigh fading channel under the average power constraint in (8), due to the arbitrarily low SNR incurred.

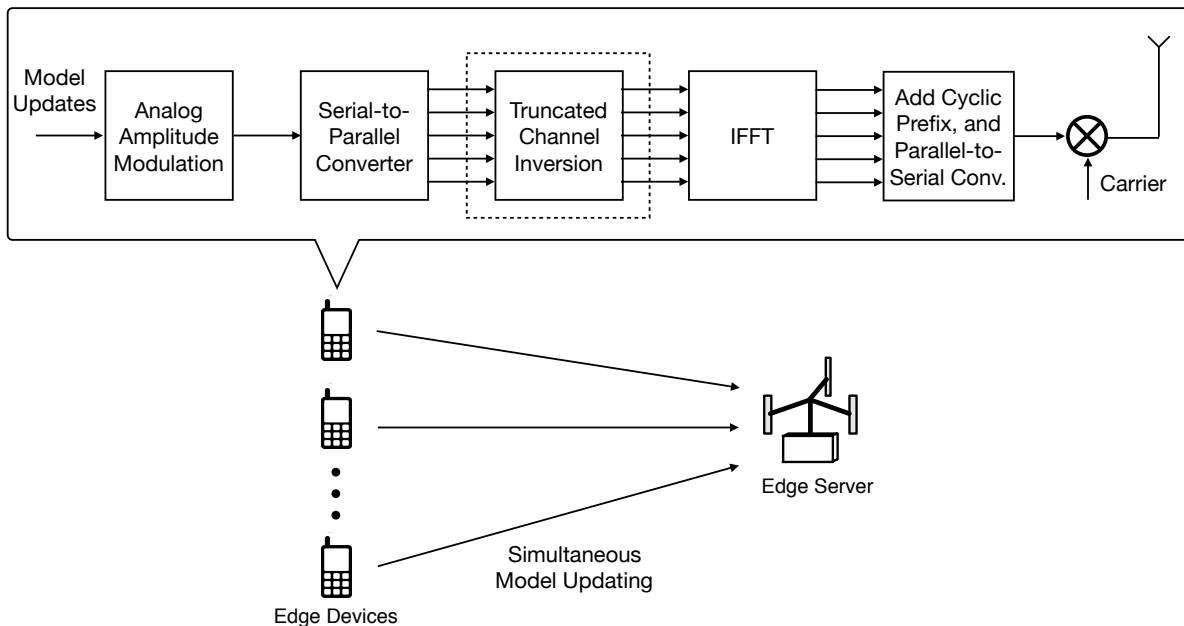


Figure 3. Transmitter design at edge devices for broadband model aggregation.

Alternatively, a better form of power adaptation is *truncated channel inversion*, which only compensates for fading above a certain *cutoff fade-depth* g_{th} ¹:

$$\text{(Truncated channel inversion)} \quad f_k = \begin{cases} \frac{\sqrt{\sigma_k}}{r_k^{-\frac{\alpha}{2}} h_k}, & |h_k|^2 \geq g_{\text{th}} \\ 0, & |h_k|^2 < g_{\text{th}}, \end{cases} \quad (11)$$

where σ_k is a scaling factor set for ensuring the average transmit power constraint in (9). As can be easily seen from (7), σ_k also determines the actual receive SNR of the k -th model-update.

With the truncated channel inversion power adaptation, the aggregated model at the edge server in (7) can be rewritten as

$$y_i = \sum_{k \in \mathcal{K}} \sqrt{\sigma_k} w_{k,i} + z, \quad \forall i, \quad (12)$$

where $\mathcal{K} = \{k \mid |h_k|^2 \geq g_{\text{th}}\}$ denotes the set of devices whose channel gains exceed the pre-defined cutoff threshold. The time and frequency indexes are omitted here for ease of notation.

To attain the desired coherent combining of the model-updates for further model averaging, the individual receive power $\{\sigma_k\}$ should be coordinated and aligned. As will be shown in Proposition 1 that the maximum receive power for a model-update is limited by the propagation distance of the link. In other words, the aligned receive power level, or equivalently the receive SNR, denoted by σ_0 , is determined by the furthest device that is subject to the severest path-loss. It follows from Proposition 1 that,

$$\text{(Receive SNR)} \quad \sigma_0 \leq \frac{P_0}{Mr_{\text{max}}^\alpha \text{Ei}(g_{\text{th}})}, \quad (13)$$

¹Here, we make the truncation decision based on only the small-scale fading so that the channel truncation ratio can be independent of the user locations. Thereby it ensures an equal chance exploitation of data distributed over different devices.

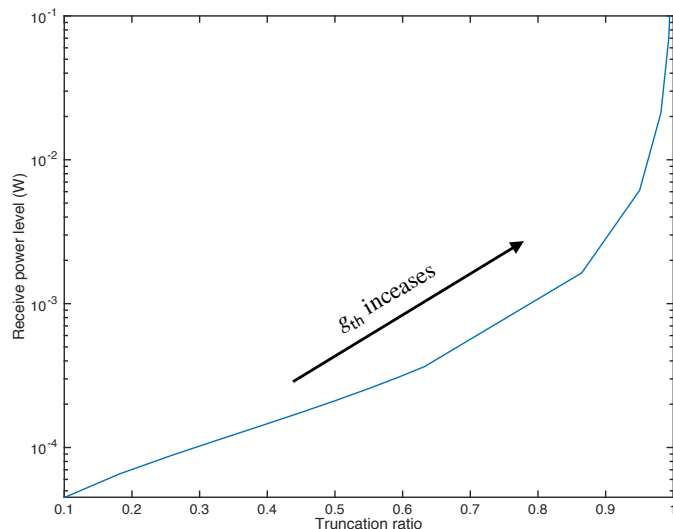


Figure 4. Illustration of the tradeoff between the receive SNR and truncation ratio of a model-update, where we set $P_0 = 1(\text{W})$, $M = 100$, $r_k = 5$, and $\alpha = 3$.

where $r_{\max} = \max_k \{r_1, r_2, \dots, r_K\}$ denotes the distance to the edge server from the furthest device.

B. Properties of Broadband Analog Aggregation

As seen in (11), the cutoff fade-depth g_{th} is the key parameter to be determined in the proposed broadband analog aggregation scheme with truncated channel inversion. Particularly, for each model-update vector, g_{th} determines the *maximum receive SNR* of the update and also its *truncation ratio*, defined by $\rho = \frac{\# \text{ of truncated coefficients}}{\# \text{ of total model-update coefficients}}$, as elaborated in the following.

First, by substituting (11) into (9), the maximum receive SNR of a model-update can be derived as a function of g_{th} as follows.

Proposition 1 (Maximum receive SNR of a model-update). For the k -th model-update with the uploading distance r_k and the selected cutoff fade-depth g_{th} , its maximum receive SNR is bounded by

$$\sigma_k \leq \frac{P_0}{M r_k^\alpha \text{Ei}(g_{\text{th}})}, \quad (14)$$

where $\text{Ei}(x)$ is the exponential integral function which is defined as $\text{Ei}(x) = \int_x^\infty \frac{1}{t} \exp(-t) dt$.

Proof: Let $g_k = |h_k|^2$ denote the channel gain of the k -th link. Since the channel coefficient is Rayleigh distributed $h_k \sim \mathcal{CN}(0, 1)$, it yields that g_k follows the exponential distribution with unit mean. Then substituting (11) into (9) gives

$$\frac{\sigma_k}{r_k^{-\alpha}} \int_{g_{\text{th}}}^\infty \frac{1}{g} \exp(-g) dg \leq \frac{P_0}{M}. \quad (15)$$

Last the desired result follows immediately by invoking the definition of the exponential integral function. ■

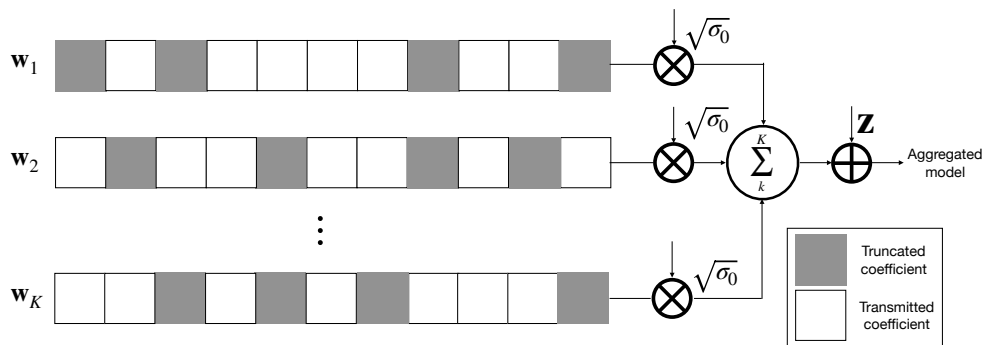


Figure 5. Illustration of signal model for analog model aggregation with truncated channel inversion policy.

As seen in (14), by setting a large cutoff fade-depth g_{th} , the truncated channel inversion power adaptation can render a high receive SNR for model-updates.

On the other hand, g_{th} also regulates the chance that the model-update coefficients got truncated and thus the completeness of the model-update. In particular, when a model-update contains sufficiently many elements, by law of large number, its truncation ratio is equal to the corresponding channel cutoff probability which is derived below.

Proposition 2 (Truncation ratio of a model-update). When the model-update dimension $p \rightarrow \infty$, the truncation ratio of a model-update is equal to the channel cutoff probability which is given by

$$\rho = \Pr(|h_k|^2 < g_{\text{th}}) = 1 - \exp(-g_{\text{th}}). \quad (16)$$

Proof: The result immediately follows from the exponential distribution of the channel gain.

Remark 1 (SNR-truncation ratio tradeoff). Combining Proposition 1 and 2, one can note that the cutoff fade-depth plays a key role in determining the quality of model-updates by controlling a tradeoff between the *receive SNR* and the *truncation ratio* of model-updates as illustrated in Fig. 4, where an increasing g_{th} trades the completeness of a model-update for a higher receive SNR and vice versa. Note that too high or too low g_{th} both harm the learning performance: the former is due to the too aggressive truncation ratio incurred, while the latter is because of the resultant weak receive SNR.

In the subsequent performance evaluation, the cutoff fade-depth will be optimized numerically to maximize the learning performance by grid search. To provide an overview of the effect of cutoff fade-depth on the aggregated model-update, a signal model showing the process of the analog model aggregation with truncated channel inversion policy is illustrated in Fig. 5.

Remark 2 (User scheduling problem in AirComp). As shown in (13), to ensure a common receive power for all model-updates, devices that are near to the edge server need to reduce its transmit power to align with the far away devices in receive power. A comparison between (13) and (14) suggests that the distance ratio between the nearby and cell-edge users determines the level of the compromised transmit power at the nearby users due to receive power alignment. Therefore, simply scheduling all the available users,

referred as *all-inclusive scheduling*, may result in a large distance ratio and thus a highly inefficient use of available power at the nearby devices. On the other hand, scheduling only the nearby users may also compromise the learning performance due to the unexploitation of the data distributed at the cell-edge. Therefore, it raises a unique tradeoff to be tackled in the user-scheduling problem for AirComp-assisted FEEL, that is to *balance the resultant receive SNR of the aggregated update and the amount of data exploited in the update computation*.

The above user scheduling problem will be tackled in the next section.

IV. OPPORTUNISTIC SCHEDULING

As mention earlier, simply scheduling all users for analog model aggregation may lead to huge penalty in SNR loss. To enhance the receive SNR on the aggregated model-updates, it is desirable to schedule only those cell-interior devices that lie close to the edge server. This is particularly appealing for the scenario where the edge devices is with high mobility and the cell-interior devices change rapidly over time. Motivated by this, in the current section, the performance of the following opportunistic scheduling scheme is investigated.

Scheme 1 (Opportunistic scheduling). The edge server schedules only the cell-interior edge devices whose distances are no larger than R_{in} .

Remark 3 (Tradeoff controlled by the cell-interior range). In the opportunistic scheduling scheme, the cell-interior range R_{in} serves as a tuning parameter that regulates the said tradeoff between *receive SNR* and the *amount of data exploited* in update computation. Essentially, the smaller R_{in} the higher receive SNR can be attained but the smaller portion of distributed data in the cell are exploited at each communication round, and vice versa. The tradeoff in turn determines the model convergence rate and the accuracy of the ultimate model converged.

In the following subsections, we will quantify the above tradeoff by deriving the expected receive SNR and the ratio of data exploited in the update computation as a function of the cell-interior range R_{in} . The ultimate learning performance of the scheme will be evaluated via experiments in Section VI.

A. Analysis on the Ratio of Data Exploited.

Assume equal data partition among all the edge devices, the ratio of data exploited in update computation is equal to the ratio of scheduled users in the cell, the derivation of which is presented in the following under the uniform device distribution network topology described in Section II-C.

Let K_{in} denote the number of devices lying in the range of R_{in} and thus scheduled. The number K_{in} is a random variable whose distribution is parameterized by R_{in} , R , and K and derived as follows.

Lemma 1 (Distribution of the number of scheduled devices). In opportunistic scheduling, given the cell-interior range R_{in} , the number of scheduled users follows a Binomial distribution with the probability mass function (PMF) given by:

$$\Pr(K_{\text{in}} = k) = \binom{K}{k} \left(\frac{R_{\text{in}}^2}{R^2}\right)^k \left(1 - \frac{R_{\text{in}}^2}{R^2}\right)^{K-k}, \quad (17)$$

Proof: See Appendix A. ■

Based on Lemma 1, one can easily obtain the expected ratio of the scheduled devices below:

Corollary 1 (Expected ratio of scheduled-devices/exploited-data). In opportunistic scheduling, given the cell-interior range R_{in} , the expected ratio of scheduled-devices (or equivalently exploited-data) is defined and given by

$$\mathbb{E}\left(\frac{K_{\text{in}}}{K}\right) = \left(\frac{R_{\text{in}}}{R}\right)^2. \quad (18)$$

B. Analysis on Expected Receive SNR

For comparison, the expected receive SNR of the all-inclusive scheduling scheme mentioned in Remark 2 is first derived, followed by that of the opportunistic scheduling scheme. Last, based on the derived results, the power gain of the opportunistic scheduling can be characterized.

1) *All-Inclusive Scheduling*: In order to derive $\mathbb{E}(\sigma_0)$ with σ_0 defined in (13), the distribution of $r_{\text{max}} = \max_k\{r_1, r_2, \dots, r_K\}$ is required which is provided as follows.

Lemma 2 (Distribution of maximum distance). The PDF of the maximum distance r_{max} under the uniform user distribution in (10) is given by

$$f_{r_{\text{max}}}(r) = \frac{2K}{R^{2K}} r^{2K-1}. \quad (19)$$

Proof: Starting from (10), the proof is straightforward and omitted here for brevity. ■

With Lemma 2 at hand, the expected receive SNR of the all-inclusive scheduling scheme can be derived as follows.

Proposition 3 (Expected receive SNR for all-inclusive scheduling). By employing all-inclusive scheduling, the resultant expected receive SNR is given by

$$\mathbb{E}(\sigma_0) = \frac{2K}{2K - \alpha} \frac{P_0}{MR^\alpha \text{Ei}(g_{\text{th}})}, \quad (20)$$

where the assumption that $2K - \alpha > 0$ is required. Since $\alpha \in [3, 4]$ in practice, the assumption can be easily satisfied by having the number of edge devices $K > 2$.

Proof: See Appendix B. ■

2) *Opportunistic Scheduling*: For opportunistic scheduling, the following key results can be derived.

Proposition 4 (Expected receive SNR for opportunistic scheduling). By employing opportunistic scheduling, the resultant expected receive SNR is given by

$$\mathbb{E}[\sigma_0(R_{\text{in}})] = \frac{c(R_{\text{in}})P_0}{MR_{\text{in}}^\alpha \text{Ei}(g_{\text{th}})}, \quad (21)$$

where $c(R_{\text{in}})$ is a bounded scaling factor depending on R_{in} and K with

$$c(R_{\text{in}}) = \sum_{k=2}^K \frac{2k}{2k-\alpha} \binom{K}{k} \left(\frac{R_{\text{in}}^2}{R^2}\right)^k \left(1 - \frac{R_{\text{in}}^2}{R^2}\right)^{K-k}.$$

Particularly, for the typical case that $\alpha = 3$, we can show that $1 \leq c(R_{\text{in}}) \leq 4$.

Proof: See Appendix C. ■

A direct comparison between Proposition 3 and 4 yields the gain in the expected receive SNR of opportunistic scheduling over the all-inclusive counterpart as presented below.

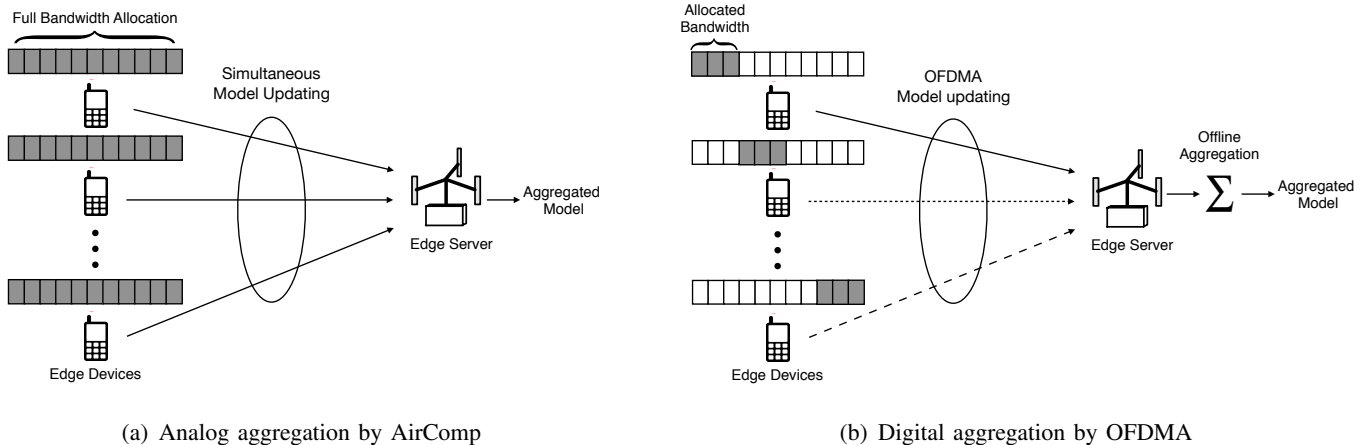
Proposition 5 (Power gain of the opportunistic scheduling). Given the cell-interior range R_{in} , the opportunistic scheduling can attain a receive SNR gain over the all-inclusive scheduling by a factor:

$$\frac{\mathbb{E}[\sigma_0(R_{\text{in}})]}{\mathbb{E}(\sigma_0)} = a \left(\frac{R}{R_{\text{in}}}\right)^\alpha, \quad (22)$$

where $a = \frac{2K-\alpha}{2K}c(R_{\text{in}})$ is a bounded scaling factor.

Remark 4 (Data-SNR tradeoff). Combining the analytical results in Corollary 1 and Proposition 5, one see that both the data-exploitation ratio and the power gain of the opportunistic scheduling is a non-linear function of the range ratio $\frac{R_{\text{in}}}{R}$ but with different exponent scalings: the former is a fixed square scaling while the scaling of the latter depends on the path-loss exponent α . Generally speaking, for a high path-loss component α , the learning performance is *noise-limited* thus it is desired to have a smaller cell-interior range R_{in} to avoid the heavy receive power penalty due to the scheduling of the far-away devices. In contrast, for a small path-loss component, the learning performance is bottlenecked by the size of training set, and thus *data-limited*. Thereby, it is preferable to increase the cell-interior range to include more distributed data to the training set with a slightly degraded receive SNR.

However a theoretical derivation of the optimal R_{in} that maximizes the learning accuracy is extremely challenging if not impossible since how the said tradeoff affect the learning performance has a complex dependence on the data distribution, learning task and the learning model used. Nevertheless, a general insight can be distilled is that, in the case of non-IID data distribution, the learning performance tends to be more data-limited and thus a larger R_{in} is desired compared with the IID case.



(a) Analog aggregation by AirComp

(b) Digital aggregation by OFDMA

Figure 6. Analog model aggregation versus digital model aggregation.

C. Alternating Scheduling between Cell-Interior and Cell-Edge Users

Purely scheduling the cell-interior user may lead to a high effective update-SNR but may suffer from exploiting only a small portion of distributed data. This is the case where the edge devices remain static during the training. As reflected in Corollary 1, far more data lie at the outer-circle of the coverage range of the edge server. The failure of exploiting the rich data lying at the cell-edge may lead to significant learning performance degradation due to the data deficiency effect. This motivates us to propose the following alternating scheduling scheme that can also make exploitation of the cell-edge data.

Scheme 2 (Alternating scheduling). The edge server alternates between the cell-interior scheduling mode (Scheme 1) and the all-inclusive scheduling mode.

In Scheme 2, the alternating frequency between the two modes might be further optimized to balance the receive SNE of the update and the amount of data exploited. The performance of Scheme 2 will be evaluated experimentally in section VI.

V. LATENCY ANALYSIS: ANALOG AGGREGATION V.S. DIGITAL AGGREGATION

As mentioned, the key advantage of the proposed broadband analog aggregation over the classic digital counterpart by OFDMA is the significant reduction in communication latency. Essentially, as illustrated in Fig. 6, the two schemes mainly differ in the how the available bandwidth are shared across different devices: the former allows the complete reuse of the bandwidth to exploit interference for direct computation, while the latter orthogonalizes the bandwidth allocation to avoid interference for reliable communication. In this section, we will provide the theoretical analysis of the the latency performance of the two schemes, from which the said latency gain achieved by the proposed broadband analog model aggregation can thus be quantified.

A. Latency Analysis of Digital Aggregation

For digital model aggregation, model parameters are first quantized into a bit sequence. Let Q denotes the number of bits used for digital representation of a model parameter. Therefore, for a device to upload a model update of dimension p , the total data amount to be transmitted is calculated as

$$\text{(Data amount for one update)} \quad D_{\text{dig}} = pQ \text{ (bits)}. \quad (23)$$

During update aggregation, all K edge devices communicate with the edge server in an OFDMA manner to avoid inter-user interference. For simplicity, we assume that the total available bandwidth is evenly divided and assigned to K devices, so each device uploads its local model via an equal portion of allocated sub-channels (see Fig. 6(b)). Thus the number of sub-channels allocated to device k is given by

$$\text{(Allocated sub-channels per device)} \quad M_k = \frac{M}{K}. \quad (24)$$

Through the allocated sub-channels, model updates from device k can be received without interference at the edge server. Thus the received signals from device k can be rewritten from (7) as

$$y_k = r_k^{-\frac{\alpha}{2}} h_k f_k x_k + z. \quad (25)$$

where the notations follow those in (7) with the time and frequency indexes omitted to avoid heavy notation. x_k denotes the digitally-modulated bit representation of the model-update coefficients. The power control factor f_k therein is subject to a more lenient average power constraint in (26) than that in (9), as each device now concentrates its transmit power on only a fraction of allocated bandwidth.

$$\text{(Power constraint)} \quad \mathbb{E} [|f_k(h_k)|^2] \leq \frac{K P_0}{M}, \quad \forall k. \quad (26)$$

In order to derive the model updating latency, the transmission rate of the system is needed. Instead of directly applying the Shannon capacity, we are interested in the practical adaptive MQAM modulation scheme and the resultant transmission rate.

Essentially, the implementation of adaptive MQAM simply involves a proper partition of the receive SNR range into several non-overlapping region and associate a region with a constellation whose order increases as the receive SNR. The optimal power control policy that maximize the spectrum efficiency of the adaptive MQAM scheme is the well-known *water filling policy*. However, the resultant transmission rate of the policy does not admit a closed-form solution [31]. As a good sub-optimal policy and also for analytical tractability, we consider the truncated channel inversion policy as shown in (11). Thus, given a target bit error rate (BER), the resultant transmission rate for device k is given by [31]:

$$\text{(Instantaneous transmission rate)} \quad R_k = \begin{cases} M_k B_{\text{sub}} \log_2 \left(1 + \frac{-1.5\sigma_k}{\ln(5\text{BER})} \right), & |h_k|^2 \geq g_{\text{th}} \\ 0, & |h_k|^2 < g_{\text{th}}, \end{cases} \quad (27)$$

where $B_{\text{sub}} = \frac{B}{M}$ denotes the sub-carrier spacing in the OFDM system; the receive SNR σ_k can be easily derived by substituting (11) into (26), which yields

$$\sigma_k = \frac{KP_0}{Mr_k^\alpha \text{Ei}(g_{\text{th}})}. \quad (28)$$

By taking expectation of (27) with respect to channel coefficient, the expected transmission rate for device k can be expressed by

$$R_k = M_k B_{\text{sub}} \log_2 \left(1 + \frac{-1.5\sigma_k}{\ln(5\text{BER})} \right) \Pr(|h_k|^2 \geq g_{\text{th}}). \quad (29)$$

According to the Rayleigh fading channel model, we have $\Pr(|h_k|^2 > g_{\text{th}}) = \exp(-g_{\text{th}})$. Thus (29) can be explicitly given by

$$\text{(Expected transmission rate)} \quad R_k = M_k B_{\text{sub}} \log_2 \left(1 + \frac{-1.5KP_0}{\ln(5\text{BER})Mr_k^\alpha \text{Ei}(g_{\text{th}})} \right) \exp(-g_{\text{th}}). \quad (30)$$

With (23) and (30) at hand, we are readily derive the expected update uploading latency for device k , denoted by T_k , as follows.

$$T_k = \frac{D_{\text{dig}}}{R_k} = \frac{KpQ}{MB_{\text{sub}} \log_2 \left(1 + \frac{-1.5KP_0}{\ln(5\text{BER})Mr_k^\alpha \text{Ei}(g_{\text{th}})} \right) \exp(-g_{\text{th}})}. \quad (31)$$

Since the model aggregation is performed offline by the edge server after all local models are reliably received, the communication latency is determined by the slowest device, which is referred to the *straggler effect*. Accordingly, we can establish the main result in the current sub-section as follows.

Proposition 6 (Expected latency for digital model aggregation). The expected model-updating latency of the broadband digital model aggregation scheme is given by

$$T_{\text{dig}} = \max_k \{T_k\} = \frac{KpQ}{M \log_2 \left(1 + \frac{-1.5KP_0}{\ln(5\text{BER})Mr_{\text{max}}^\alpha \text{Ei}(g_{\text{th}})} \right) \exp(-g_{\text{th}})} T_s, \quad (32)$$

where $r_{\text{max}} = \max_k \{r_1, r_2, \dots, r_K\}$ denotes the distance to the furthest user, and $T_s = \frac{1}{B_{\text{sub}}}$ is the symbol duration of an OFDM symbol.

Several key observations can be made from (32) as summarized below:

- The latency of the scheme approximately linearly scales with the number of accessing devices K .
- Due to the straggler effect, the latency of the scheme is bottlenecked by the distance to the furthest user in the network r_{max} . The strength of the latency penalty for scheduling a far-away user is determined by the path-loss exponent α .
- The latency can be controlled by the target reliability guarantee specified by the BER. Lower BER can accelerate the update aggregation process and vice versa.

B. Latency Analysis of Analog Model Aggregation

For analog model aggregation, each model parameters are amplitude-modulated to a single analog symbol and each sub-channel is dedicated for a single parameter transmission. Thus, to upload a model update of dimension p , the total number of analog symbols to be transmitted is calculated as

$$\text{(Analog symbols for one update)} \quad D_{\text{ana}} = p \text{ (symbols)}. \quad (33)$$

Since all devices transmit their model-updates simultaneously on the whole available sub-channels. One can easily derive that the number of OFDM symbols involved for the whole updating is equal to $\frac{p}{M}$. Thus, we establish the following key result.

Proposition 7 (Latency for analog model aggregation). The model-updating latency of the broadband analog model aggregation scheme is given by

$$T_{\text{ana}} = \frac{p}{M} T_s. \quad (34)$$

Two key observations can be made from the result in (34) as follows:

- Due to the complete reuse of radio resource (e.g., time and frequency) in the analog aggregation, the resultant latency is thus independent of the number of accessing devices, making it particularly promising in large-scale edge learning network.
- The latency of the analog aggregation is a deterministic value independent of the channel realizations, which is in contrast to the digital counterpart whose latency is a random variable due to the channel-dependent transmission rate shown in (27).

C. Latency Comparison between Analog and Digital Aggregation

Combining Proposition 6 and 7, we are ready to establish the latency gain of analog aggregation over digital one, defined as $\eta = \frac{T_{\text{dig}}}{T_{\text{ana}}}$, as follows.

Proposition 8 (Latency gain). The latency gain of the analog aggregation over its digital counterpart, measured by their latency ratio, is given by

$$\gamma = \frac{KQ}{\log_2 \left(1 + \frac{-1.5KP_0}{\ln(5\text{BER})M r_{\text{max}}^\alpha \text{Ei}(g_{\text{th}})} \right) \exp(-g_{\text{th}})}. \quad (35)$$

Based on (8), the following insights can be distilled.

- The latency gain linearly scales with the quantization resolution Q and approximately linearly scales with the network scale K . More precisely, we have the following scaling law with respect to K :

$$\gamma = O\left(\frac{K}{\log_2 K}\right), \quad K \rightarrow \infty. \quad (36)$$

- The latency gain can keep increasing unboundedly as $r_{\text{max}} \rightarrow \infty$ and the increasing rate is highly dependent on the path-loss exponent α .

Table I
COMPARISON BETWEEN ANALOG AND DIGITAL MODEL AGGREGATION.

	Analog model aggregation	Digital model aggregation
Effect of channel condition	Truncation ratio and receive SNR [see (14) & (16)]	Transmission rate [see (27)]
Inter-user dependency	Receive SNR depends on furthest user [see (13)]	Latency depends on furthest user [see (32)]
Latency scaling with # of user	Independent [see (34)]	Approximately linear scaling [see (32)]
Update reliability guarantee	Less strict guarantee by scheduling [see (22)]	Strict guarantee specified by BER

- The latency gain is a decreasing function of the target BER. Particularly, as $\text{BER} \rightarrow 0$, the latency gain grows unboundedly, i.e., $\gamma \rightarrow \infty$, since no practical modulation scheme can attain zero BER.
- The (digital scheme) cutoff fade-depth has contrary effects on the latency gain via affecting the receive SNR and channel-cutoff probability of the digital scheme. On one hand, increasing g_{th} leads to a higher receive SNR of the digital scheme as reflected in (28) that reduces the latency gain. On the other hand, a large g_{th} also incurs a high channel-cutoff probability that reduces the expected transmission rate of the digital scheme (see (30)), resulting in a higher latency gain.

A comprehensive comparison between analog and digital aggregation is summarized in Table I.

VI. EXPERIMENT RESULTS

A. Experiment Settings

Consider a FEEL system with one edge server and $K = 200$ edge devices. The simulation parameters are set as follows unless specified otherwise. The cell radius is $R = 100$, the path loss exponent $\alpha = 3$, the number of sub-channels $M = 1000$, and the average transmit-SNR constraint, defined as $\rho_t = \frac{P_0}{N_0}$, is set to be 20 dB.

For exposition, we consider the learning task of handwritten-digit recognition using the well-known MNIST dataset that consists of 10 categories ranging from digit “0” to “9” and a total of 60000 labeled training data samples. To simulate the distributed mobile data, we consider two types of data partitions, i.e., **i.i.d.** setting and **non-i.i.d.** one. For the former setting, we randomly partition the training samples into 200 equal shares, each of which is assigned to one particular device. While for the latter setting, we first sort the data by digit label, divide it into 400 shards of size 150, and assign each of 200 clients 2 shards. As illustrated in Fig. 7, the classifier model is implemented using a 6-layer convolutional neural network (CNN) that consists of two 5x5 convolution layers ReLu activation (the first with 32 channels, the second with 64), each followed with 2x2 max pooling, a fully connected layer with 512 units and ReLu activation, and a final softmax output layer (582,026 parameters in total).

B. Tradeoff in User Scheduling

The tradeoff inherent in the user scheduling problem is first shown in Fig. 8. Consider the opportunistic scheduling in Scheme 1. The bar-figure showing the ultimate test accuracy of the learned model against the selection of the cell-interior range R_{in} normalized by the cell-radius R is plotted under varying values

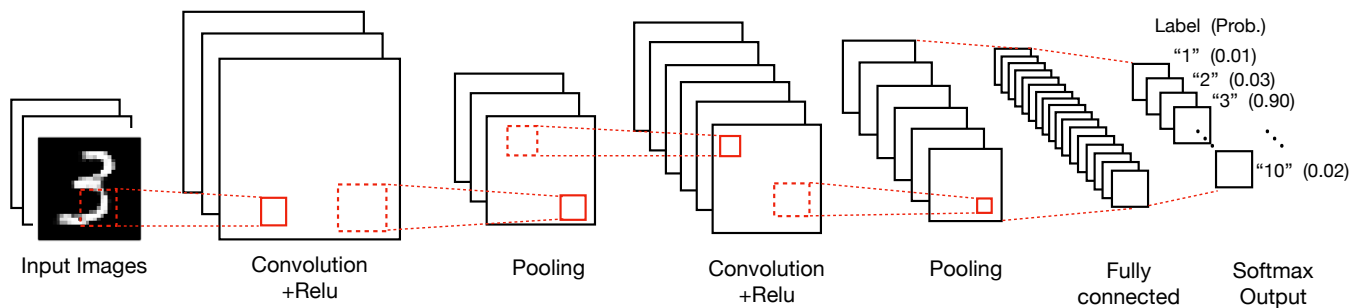


Figure 7. Architecture of convolutional neural network

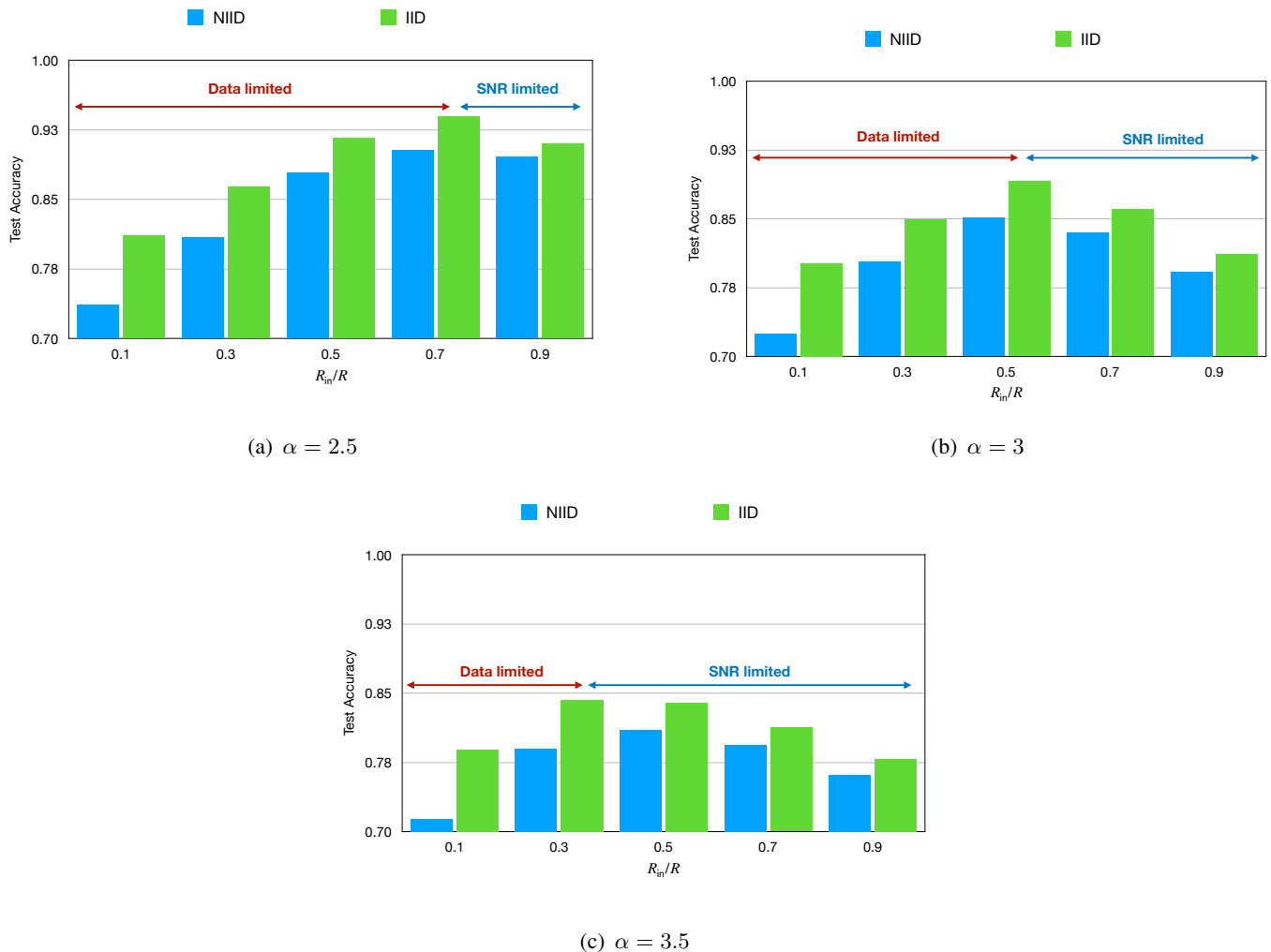
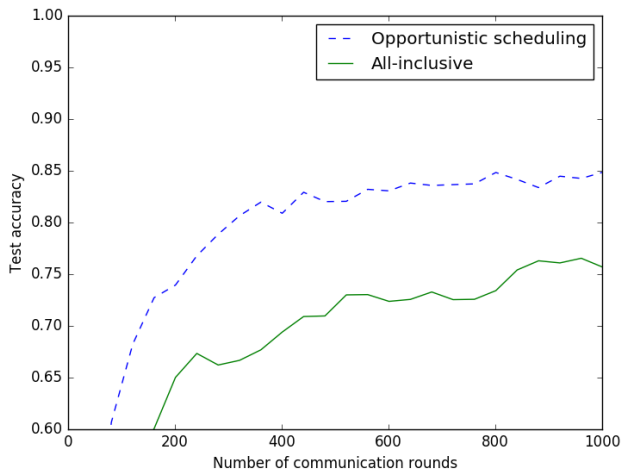
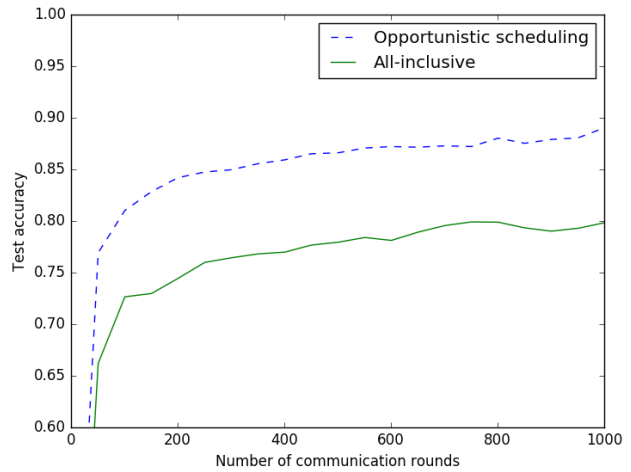


Figure 8. Test accuracy versus cell-interior range in opportunistic scheduling.

of the path-loss component α . Both the cases of i.i.d and non-i.i.d data-partition are experimented. It can be observed from all plots that, as the more devices included in the aggregation by increasing R_{in} , the test accuracy first increases then decreases after a certain point, passing through a data-limited regime towards a SNR-limited regime. The phenomenon verifies the existence of the said data-SNR tradeoff in user scheduling. In addition, as the path-loss exponent increases, the learning performance is found to be more suffered from SNR-limited than data-limited, suggesting a decreasing choice of R_{in} to reduce the

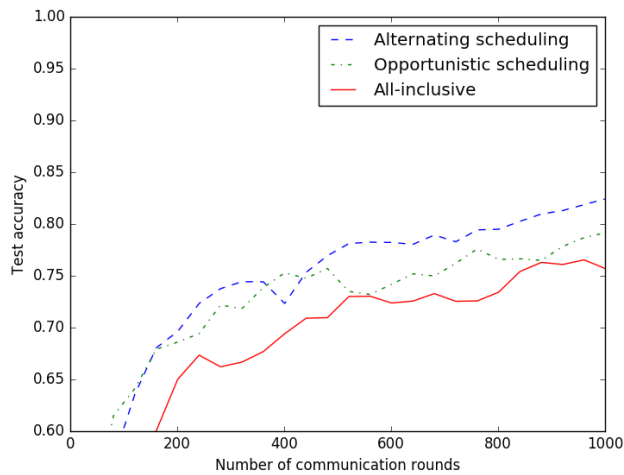


(a) NIID data distribution

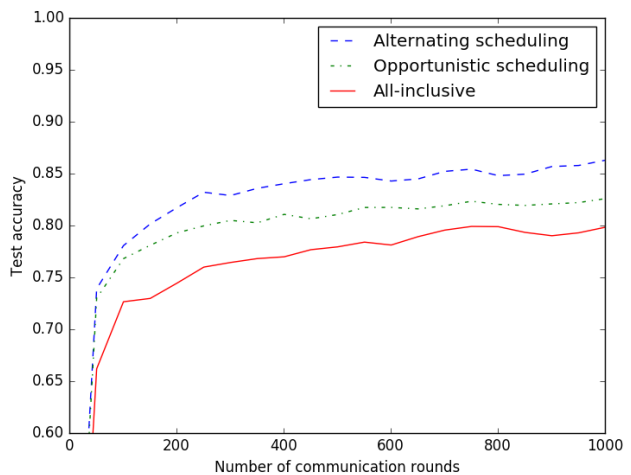


(b) IID data distribution

Figure 9. Performance comparison between different scheduling schemes in the high-mobility scenario.



(a) NIID data distribution



(b) IID data distribution

Figure 10. Performance comparison between different scheduling schemes in the low-mobility scenario.

SNR penalty due to the scheduling of far-away users. Last, it is also noted that the non-i.i.d. setting is in general more data-hungry than the i.i.d. setting, thus preferring a higher value of R_{in} even when the path-loss exponent is high (see Fig. 8(c)). The observations align with our discussions in Remark 4.

C. Performance of Opportunistic Scheduling

The performance of the developed opportunistic scheduling scheme is evaluated in Fig. 9 and 10, targeting the high-mobility and low-mobility networks, respectively. The difference between the two scenarios is that, in the former setting, the devices lying within the cell-interior change rapidly over communication rounds, while in the latter case, the device location remains unchanged throughout the entire learning process. For all curves, the cell-interior range parameter R_{in} is optimized numerically for the best test accuracy. It is observed that the opportunistic scheduling outperforms the naive all-inclusive scheme by a remarkable gap in the high mobility setting where the learning performance is more SNR-

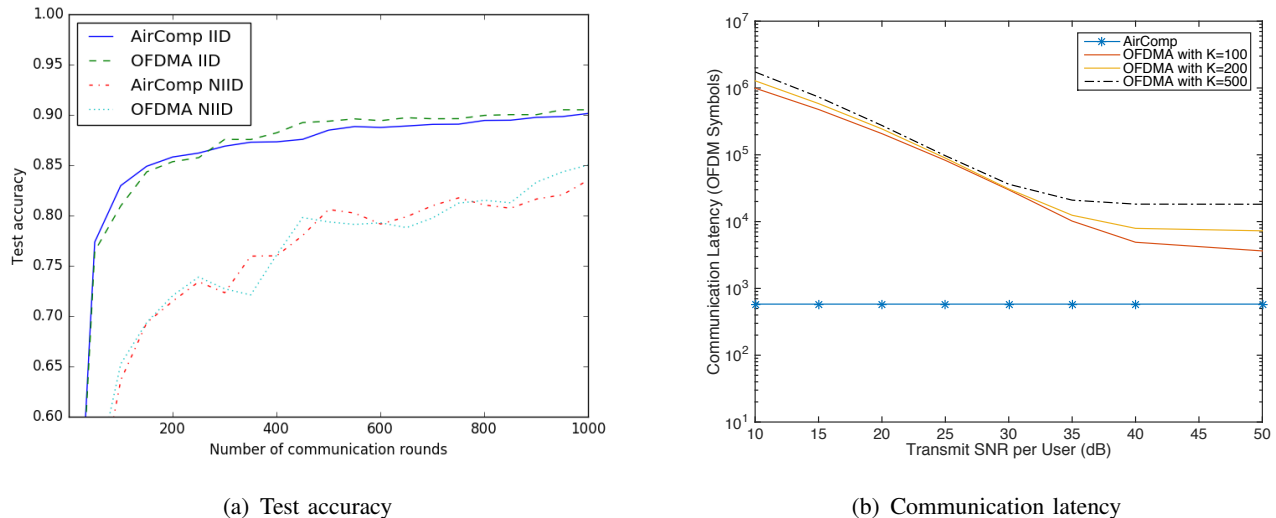


Figure 11. Performance comparison between AirComp and OFDMA.

limited. On the other hand, in the low mobility setting where the opportunistic scheduling suffers from data-deficiency, the proposed alternating scheduling scheme can enhance the learning performance further by occasionally exploiting the data in the cell-edge devices.

D. Performance Comparison: Analog Aggregation v.s. Digital Aggregation

The learning accuracy and communication latency of the analog aggregation based on AirComp and the digital one based on OFDMA are compared in Fig. 11 under the same transmit SNR per user and a fixed user scheduling scheme with $\frac{R_{in}}{R} = 0.5$. For the digital scheme, model-update coefficients are quantized into bit sequence with 16-bit per coefficient, and the adaptive MQAM modulation is used to maximize the spectrum efficiency under a target BER of 10^{-3} . As shown at Fig. 11(a), although AirComp is expected to be more vulnerable to channel noise, it is interesting to see that the two schemes are comparable in learning accuracy (for both the i.i.d. and non-i.i.d. settings). Such accurate learning of AirComp is partly due to the high expressiveness of the deep neural network which makes the learnt model robust against perturbation by channel noise. The result has a profound and refreshing implication that reliable communication may not be the primary concern in edge learning. Essentially, AirComp exploits this relaxation on communication reliability to trade for a low communication latency as shown at Fig. 11(b). The latency gap between the two schemes is remarkable. Without compromising the learning accuracy, AirComp can achieve a significant latency reduction ranging from 10x to 1000x. In general, the superiority in latency of AirComp over OFDMA is more pronounced in the low SNR regime and dense-network scenarios.

VII. FURTHER DISCUSSION

A. Power Equalization by AirComp Beamforming

It is worth pointing out that the proposed broadband analog aggregation scheme can be further enhanced by beamforming technique if multi-antenna array is available at the edge server. The key idea is to form

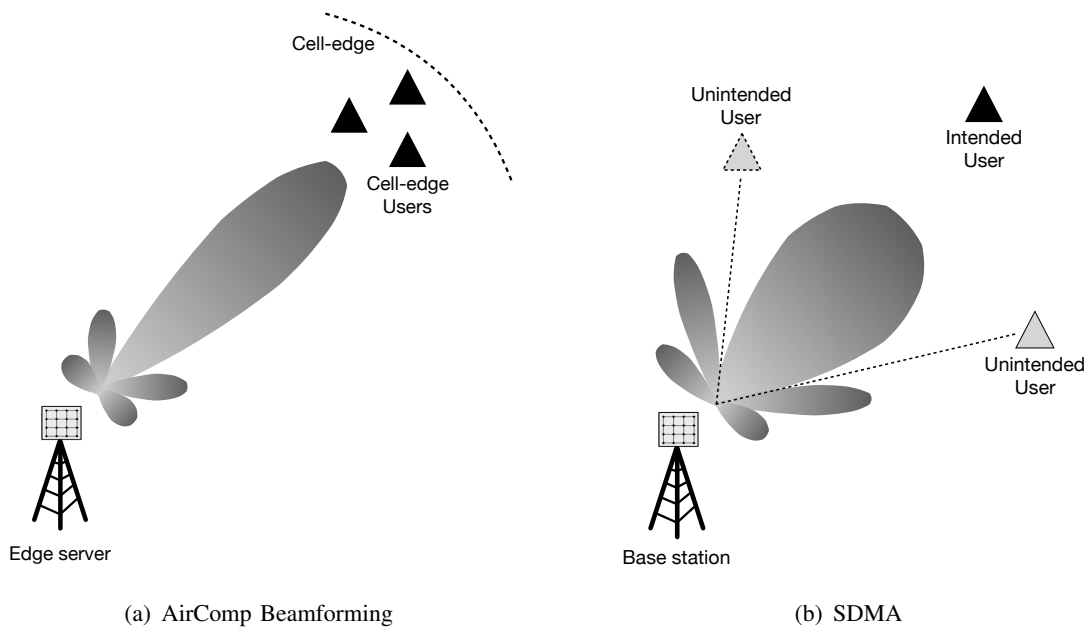


Figure 12. Illustration of AirComp beamforming and SDMA.

sharp beams towards those cell-edge devices to compensate their path-loss so that the receive SNR in (13) bottlenecked by the furthest devices can be improved.

The resultant AirComp-beamforming for weak-user enhancement is in sharp contrast with the conventional space division multiple access (SDMA) beamforming in design principle. Essentially, AirComp-beamforming tends to equalize different users' receive power to better exploit "interference" for computation, while SDMA is to suppress multi-user interference so as to recover individual data streams from different devices. The difference can be noted more clearly in their problem formulation.

To this end, we consider the following multi-antenna system model:

$$\mathbf{y} = \mathbf{F}^H \mathbf{H} \mathbf{x} + \mathbf{F}^H \mathbf{n}, \quad (37)$$

where $\mathbf{F} \in \mathbb{C}^{N \times K}$ is the beamforming matrix to be designed and N denotes the number of antennas equipped at the edge server; $\mathbf{H} \in \mathbb{C}^{N \times K}$ is the channel matrix whose k -th column represents the channel vector for the k -th device. $\mathbf{x} \in \mathbb{C}^K$ is the transmitted symbol vector with the k -th element being the symbol from the device k . \mathbf{n} is the AWGN vector with $E(\mathbf{n}\mathbf{n}^H) = N_0 \mathbf{I}$.

According to (37), the AirComp beamforming for weak-user enhancement can be designed by solving the following *unconstrained SNR maximization* problem:

$$\text{(AirComp beamforming)} \quad \max_{\mathbf{F}} \frac{\text{Tr}(\mathbf{F}^H \tilde{\mathbf{H}} \tilde{\mathbf{H}}^H \mathbf{F})}{N_0 \text{Tr}(\mathbf{F}^H \mathbf{F})}, \quad (38)$$

where $\tilde{\mathbf{H}}$ contains the channel vectors of the weak users to be enhanced.

On the other hand, in SDMA, each column of \mathbf{F} , denoted by \mathbf{f}_k , represents a dedicated beam targeting an intended user while nulling the interference from others. It thereby yields the following *constrained*

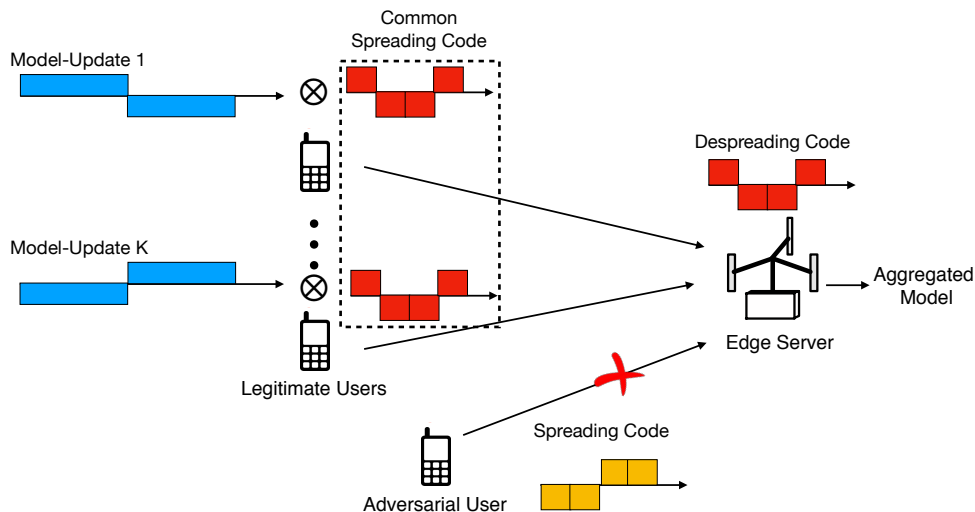


Figure 13. Illustration of robust analog model aggregation by direct sequence spread spectrum technique.

SNR-maximization problem.

$$\begin{aligned}
 \text{(SDMA beamforming)} \quad & \max_{\mathbf{f}_k} \frac{\mathbf{f}_k^H \mathbf{h}_k}{\sum_{g \neq k} \mathbf{f}_k^H \mathbf{h}_g + N_0} \quad \forall k \\
 \text{s.t.} \quad & \mathbf{f}_k^H \mathbf{h}_g = 0, \quad \forall g \neq k.
 \end{aligned} \tag{39}$$

Remark 5 (Feasibility condition). A comparison between the problem in (38) and that in (39) reveals that, the implementation of SDMA requires $N \geq K$ to ensure there are sufficient DoFs to enforce the zero-forcing constraints. This may not be feasible for the large-scale IoT network with a large K , e.g., 100 – 1000. In contrast, the AirComp beamforming is always feasible while more DoFs can lead to a higher SNR enhancement to the weak users.

Remark 6 (Beam pattern comparison). The resultant beamformer patterns from the two formulations are compared in Fig.12. In general, AirComp beamforming can form sharper and stronger beams towards the targeted cell-edge users as the full DoFs are used for SNR enhancement. On the contrary, the beams formed by SDMA towards the intended users tend to be flatter and weaker as the interference nulling constraints consume part of the DoFs, leaving only a fraction of DoFs for SNR enhancement. Furthermore, users with similar spatial signatures (channel vectors) may cause differentiability issue in SDMA, especially when N is not large enough and thus low spatial resolution of the resultant beams. This, however, makes no trouble to AirComp beamforming design as no discrimination between users is required.

B. Robust Design Against Adversarial Attack by Spectrum Spread

One practical issue to be concerned in the federated edge learning is the vulnerability to the adversarial attack by some hostile users who purposely upload inaccurate model-updates or random noise during the model aggregation. The attack may lead to the divergence of the learning algorithm and thus crash down the whole training process. This motivates the development of robust design that can distinguish and suppress the attack from adversarial users as discussed in the current subsection.

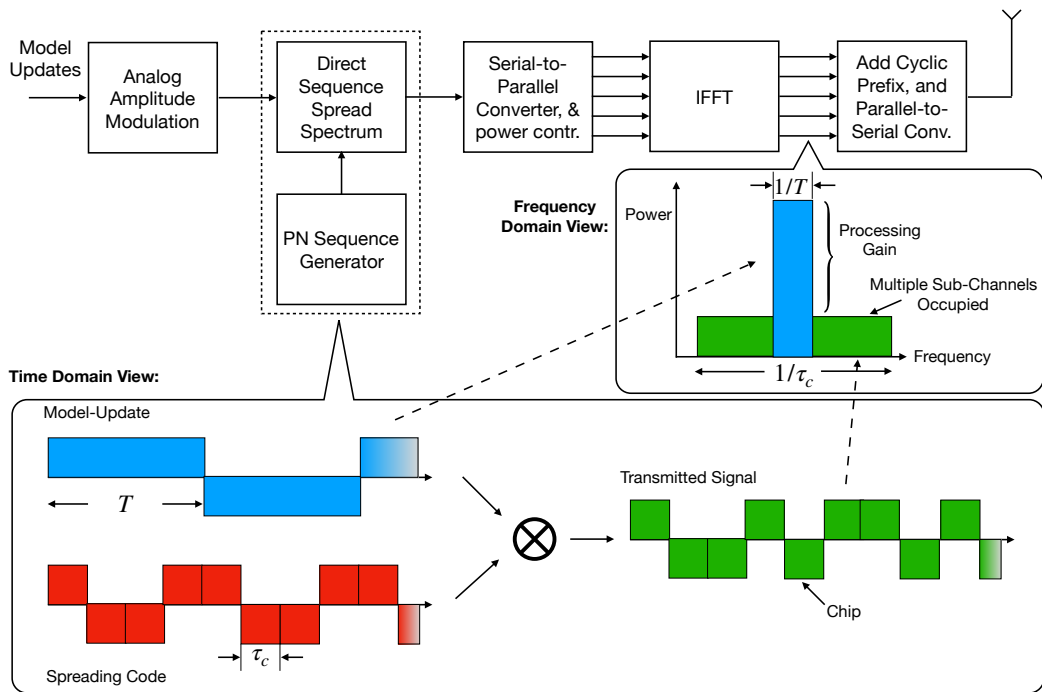


Figure 14. System architecture of DSSS-based analog model aggregation.

One potential solution of particular interest is to employ the celebrated *direct sequence spread spectrum* (DSSS) technique to encode the model-updates before transmission. As illustrated in Fig. 13, the basic idea of the design is to ensure all legitimate users to use a common assigned spreading code to facilitate model aggregation. While the adversarial user who is not aware of the assigned spreading code can be distinguished from the legitimate ones in the code domain. The main signalling protocol of the design is summarized as follows.

DSSS-based analog model aggregation:

- 1) At the beginning, all legitimate users in the network will be assigned a common spreading code, i.e., a *pseudorandom-noise* (PN) code sequence taking value 1 or -1 , which is known at the edge server but not at the adversarial user.
- 2) Then, before transmission, all legitimate users will multiply its model-update symbols with the assigned spreading code, while the adversarial user may multiply its attack with a different one.
- 3) Last, at the edge server side, the received signal aggregating all simultaneous transmitting signals will be despread using known legitimate spreading code.

Since all legitimate users share the common spreading code, the de-spreading operation on the aggregated received signal at the edge server can automatically yield the desired superposition of the original model-updates from the legitimate users while suppressing that from the adversarial user due to the mismatch in the spreading code used. In general, the longer spreading code sequence used the better suppression can be made to the adversarial attack, since the correlation between two arbitrary sequence dramatically decreases as sequence dimension grows.

The system architecture implementing the idea is depicted in Fig. 14. Compared with the original architecture shown in Fig. 3, the implementation of DSSS simply involves adding an additional block between the analog amplitude modulation and the IFFT block. As illustrated, the multiplication between the model-update with a high-rate spreading code in the time domain is equal to spreading the bandwidth used for transmitting a model-update coefficient by a factor of

$$\text{(Spreading factor)} \quad \gamma = \frac{T}{\tau_c}, \quad (40)$$

where T denotes the symbol duration of the original model-update and τ_c the duration of a *chip*.

Essentially, the spreading factor in (40) controls a tradeoff between the latency gain of the analog aggregation scheme and the enhancement in receive SNR of model-updates as elaborated below.

Remark 7 (Latency gain v.s. SNR enhancement). As shown in Fig. 14, by using DSSS technique, the system consumes γ -times more bandwidth for the transmission of each model-update coefficient. This, to some extent, compromise the latency gain achieved by the analog model aggregation compared with the digital counterpart. Nevertheless, the cost is paid back by an additional reward: after the despreading of the aggregated signals, an processing gain of γ on the aggregate-signal power can be attained. This substantially enhances the receive SNRs of the aggregated model-updates and provides a stronger protection against the channel noise, overcoming the key weakness of analog model aggregation.

VIII. CONCLUDING REMARKS

In this paper, we have presented the framework of low-latency analog aggregation for FEEL. The design exploits the wave-from superposition property of a MAC for communication-efficient update aggregation. To compensate the undesired channel weighting on the model-updates, truncated channel inversion power adaptation policy is employed. Particularly, to align the receive power for the cell-centric and cell-edge users, a user scheduling problem, with a unique tradeoff between the resultant receive SNR and the data-exploitation ratio during learning, is identified. An opportunistic scheduling solution giving a flexible control of the above tradeoff is proposed and the performance of which is characterized. Furthermore, the latency gain of the developed analog model aggregation solution of the conventional orthogonal multiple access scheme is also derived in closed-form, providing useful guidelines on the practical system design when implementing the developed solution.

The current work opens several directions for further investigation. One direction is to further enhance the performance of the current design. In particular, clustering structure in the user location distribution can be exploited in the user scheduling to improve the performance of model aggregation. Another interesting direction is to apply the broadband AirComp design to other IoT-related applications such as high-mobility UAV networks or cloud coordinated vehicular platooning.

APPENDIX

A. Proof of Lemma 1

By definition, we can establish the following event equivalence.

$$\Pr(K_{\text{in}} = k) = \Pr(k \text{ users lie in the range of } R_{\text{in}} \text{ while } (K - k) \text{ users out of the range of } R_{\text{in}}). \quad (41)$$

Since the user-locations are i.i.d. distributed, the events defined on the right hand side in (41) follows a Binomial distribution with the success probability equal to $\Pr(r_k \leq R_{\text{in}})$, i.e., the probability that a user lie in the range of R_{in} :

$$\Pr(K_{\text{in}} = k) = \binom{K}{k} [\Pr(r_k \leq R_{\text{in}})]^k [1 - \Pr(r_k \leq R_{\text{in}})]^{K-k}. \quad (42)$$

Then, according to the uniform distribution presented in (10), we have

$$\Pr(r_k \leq R_{\text{in}}) = \int_0^{R_{\text{in}}} \frac{2r}{R^2} dr = \frac{R_{\text{in}}^2}{R^2}. \quad (43)$$

Thereby, by substituting (43) into (42), the desired result is obtained.

B. Proof of Proposition 3

By involving Lemma 2 and (13), the expected receive SNR is of the all-inclusive scheme can be computed by

$$\begin{aligned} \mathbb{E}(\sigma_0) &= \int_0^R \frac{P_0}{Mx^\alpha \text{Ei}(g_{\text{th}})} f_{r_{\text{max}}}(x) dx \\ &= \frac{P_0}{M \text{Ei}(g_{\text{th}})} \frac{2K}{R^{2K}} \int_0^R x^{2K-\alpha-1} dx \end{aligned} \quad (44)$$

To ensure that the integral in (44) converges, it requires that $2K - \alpha - 1 \geq 0$. The assumption always holds in practice as mentioned earlier. Under the assumption for convergence, by completing the integral, we can have

$$\mathbb{E}(\sigma_0) = \frac{2K}{2K - \alpha} \frac{P_0}{MR^\alpha \text{Ei}(g_{\text{th}})}, \quad (45)$$

which completes the proof.

C. Proof of Proposition 4

For the opportunistic scheduling, the expectation on the receive SNR is more challenging to derive, as the number of scheduled devices is now a random variable, adding an additional layer of randomness to the receive SNR besides the randomly distributed device-distance.

To overcome the challenge, we find it convenient to tackle the two-layer randomness sequentially using the trick of conditional expectation. Particularly, the expected aligned received power can be computed using the following formula.

$$\mathbb{E}(\sigma_0) = \mathbb{E}[\mathbb{E}(\sigma_0 | K_{\text{in}} = k)], \quad (46)$$

where the first expectation is taken over the k -furthest distance to the edge server conditioned on $K_{\text{in}} = k$, while the second expectation is over the variable K_{in} whose distribution is given in Lemma 1. Thus (46) can be explicitly written as

$$\mathbb{E}(\sigma_0) = \sum_{k=0}^K \mathbb{E}(\sigma_0 \mid K_{\text{in}} = k) \Pr(K_{\text{in}} = k). \quad (47)$$

For simplicity, we consider the typical case that $\alpha = 3$. Note that the first term in (46) is equal to zero, i.e., $\mathbb{E}(\sigma_0 \mid K_{\text{in}} = 0) = 0$, and the second term is negligible when K is sufficiently large since $\Pr(K_{\text{in}} = 1) \rightarrow 0$ and $\mathbb{E}(\sigma_0 \mid K_{\text{in}} = k)$ should be bounded.

Then remaining task is to compute $\mathbb{E}(\sigma_0 \mid K_{\text{in}} = k)$ for $k \geq 2$. Note that given $K_{\text{in}} = k$, the k scheduled devices also follow i.i.d. uniform distribution over the cell-interior with the range of R_{in} . As a result, by following similar steps in the proof of Proposition 3, for $k \geq 2$, one can easily derive that,

$$\mathbb{E}(\sigma_0 \mid K_{\text{in}} = k) = \frac{2k}{2k - \alpha} \frac{P_0}{MR_{\text{in}}^\alpha \text{Ei}(g_{\text{th}})}, \quad (48)$$

Substituting (48) into (47), it follows that

$$\mathbb{E}(\sigma_0) = \frac{P_0}{MR_{\text{in}}^\alpha \text{Ei}(g_{\text{th}})} \underbrace{\sum_{k=2}^K \frac{2k}{2k - \alpha} \binom{K}{k} \left(\frac{R_{\text{in}}^2}{R^2}\right)^k \left(1 - \frac{R_{\text{in}}^2}{R^2}\right)^{K-k}}_{c(R_{\text{in}})}, \quad (49)$$

which gives the derived result in (21).

Also note that the scaling factor $c(R_{\text{in}})$ is essentially a weighted average for the term $\frac{2k}{2k - \alpha}$ from $k = 2$ to K . Given that $\alpha = 3$, and K is sufficiently large, we note that $\frac{2k}{2k - \alpha}$ monotonically ranges from 1 to 4. Since a weighted average for the values from a range will not exceed the range, it gives the conclusion that $1 \leq c(R_{\text{in}}) \leq 4$, which completes the proof.

REFERENCES

- [1] N. Poggi, "3 key internet of things trends to keep your eye on in 2017," [Online]. Available: <https://preyproject.com/blog/en/3-key-internet-of-things-trends-to-keep-your-eye-on-in-2017/>, 2017.
- [2] G. Zhu, D. Liu, Y. Du, C. You, J. Zhang, and K. Huang, "Towards an intelligent edge: Wireless communication meets machine learning," [Online]. Available: <https://arxiv.org/abs/1809.00343>, 2018.
- [3] Y. Mao, C. You, J. Zhang, K. Huang, and K. B. Letaief, "A survey on mobile edge computing: The communication perspective," *IEEE Commun. Surveys and Tutorials*, vol. 19, pp. 2322–2358, Aug. 2017.
- [4] S. Wang, T. Tuor, T. Salonidis, K. K. Leung, C. Makaya, T. He, and K. Chan, "When edge meets learning: Adaptive control for resource-constrained distributed machine learning," in *Proc. IEEE Int. Conf. Comput. Commun. (INFOCOM)*, (Honolulu, USA), 2018.
- [5] M. I. Jordan, J. D. Lee, and Y. Yang, "Communication-efficient distributed statistical inference," *Journal of the American Statistical Association*, vol. DOI: 10.1080/01621459.2018.1429274, Feb. 2018.
- [6] H. B. McMahan, E. Moore, D. Ramage, S. Hampson, and B. A. y Arcas, "Communication-efficient learning of deep networks from decentralized data," in *International conference on Artificial Intelligence and Statistics (AISTATS)*, (Fort Lauderdale, Florida), Apr. 2017.
- [7] J. Konečný, H. B. McMahan, F. X. Yu, P. Richtárik, A. T. Suresh, and D. Bacon, "Federated learning: Strategies for improving communication efficiency," [Online]. Available: <https://arxiv.org/abs/1610.05492>, 2017.

- [8] J. Chen, X. Pan, R. Monga, S. Bengio, and R. Jozefowicz, "Revisiting distributed synchronous sgd," [Online]. Available: <https://arxiv.org/abs/1604.00981>, 2017.
- [9] R. Tandon, Q. Lei, A. G. Dimakis, and N. Karampatziakis, "Gradient coding: Avoiding stragglers in distributed learning," in *International Conference on Machine Learning (ICML)*, (Sydney, Australia), Aug. 2017.
- [10] M. Kamp, L. Adilova, J. Sicking, F. Hüger, P. Schlicht, T. Wirtz, and S. Wrobel, "Efficient decentralized deep learning by dynamic model averaging," [Online]. Available: <https://arxiv.org/abs/1807.03210>, 2018.
- [11] T. Chen, G. B. Giannakis, T. Sun, and W. Yin, "Lag: Lazily aggregated gradient for communication-efficient distributed learning," in *Conference on Neural Information Processing Systems (NIPS)*, (Montreal, CANADA), Dec. 2018.
- [12] A. F. Aji and K. Heafield, "Sparse communication for distributed gradient descent," in *Conference on Empirical Methods in Natural Language Processing (EMNLP)*, (Copenhagen, Denmark), Sep. 2017.
- [13] Y. Lin, S. Han, H. Mao, Y. Wang, and W. J. Dally, "Deep gradient compression: Reducing the communication bandwidth for distributed training," in *International conference on learning representation (ICLR)*, (Vancouver, Canada), May 2018.
- [14] B. Nazer and M. Gastpar, "Computation over multiple-access channels," *IEEE Trans. Inf. Theory*, vol. 53, pp. 3498–3516, Oct. 2007.
- [15] M. Gastpar, "Uncoded transmission is exactly optimal for a simple Gaussian sensor network," *IEEE Trans. Inf. Theory*, vol. 54, pp. 5247–5251, Nov 2008.
- [16] A. B. Wagner, S. Tavildar, and P. Viswanath, "Rate region of the quadratic Gaussian two-encoder source-coding problem," *IEEE Trans. Inf. Theory*, vol. 54, pp. 1938–1961, May 2008.
- [17] R. Soundararajan and S. Vishwanath, "Communicating linear functions of correlated Gaussian sources over a MAC," *IEEE Trans. Inf. Theory*, vol. 58, pp. 1853–1860, March 2012.
- [18] J. J. Xiao, S. Cui, Z. Q. Luo, and A. J. Goldsmith, "Linear coherent decentralized estimation," *IEEE Trans. Signal Process.*, vol. 56, pp. 757–770, Feb 2008.
- [19] M. Goldenbaum and S. Stanczak, "On the channel estimation effort for analog computation over wireless multiple-access channels," *IEEE Wireless Commun. Lett.*, vol. 3, pp. 261–264, June 2014.
- [20] C. H. Wang, A. S. Leong, and S. Dey, "Distortion outage minimization and diversity order analysis for coherent multiaccess," *IEEE Trans. Signal Process.*, vol. 59, pp. 6144–6159, Dec 2011.
- [21] M. Goldenbaum, S. Stańczak, and H. Boche, "On achievable rates for analog computing real-valued functions over the wireless channel," in *2015 IEEE International Conference on Communications (ICC)*, pp. 4036–4041, June 2015.
- [22] O. Abari, H. Rahul, and D. Katabi, "Over-the-air function computation in sensor networks," *CoRR*, vol. abs/1612.02307, 2016.
- [23] M. Goldenbaum and S. Stanczak, "Robust analog function computation via wireless multiple-access channels," *IEEE Trans. Commun.*, vol. 61, pp. 3863–3877, Sep. 2013.
- [24] O. Abari, H. Rahul, D. Katabi, and M. Pant, "Airshare: Distributed coherent transmission made seamless," in *Proc. IEEE Conference on Computer Communications (INFOCOM)*, pp. 1742–1750, Apr. 2015.
- [25] G. Zhu and K. Huang, "MIMO over-the-air computation for high-mobility multi-modal sensing," to appear in *IEEE IoT Journal*, 2018.
- [26] X. Li, G. Zhu, Y. Gong, and K. Huang, "Wirelessly powered data aggregation for IoT via over-the-air functional computation: Beamforming and power control," submitted to *IEEE Trans. Wireless Commun.* [Online]. Available: <https://arxiv.org/pdf/1808.04616.pdf>, 2018.
- [27] D. Wen, G. Zhu, and K. Huang, "Reduced-dimension design of MIMO over-the-air computing for data aggregation in clustered IoT networks," submitted to *IEEE Trans. Wireless Commun.* [Online]. Available: <https://arxiv.org/pdf/1812.02373.pdf>, 2018.
- [28] B. Nazer and M. Gastpar, "Compute-and-forward: Harnessing interference through structured codes," *IEEE Trans. Inf. Theory*, vol. 57, pp. 6463–6486, Oct. 2011.
- [29] A. Sakzad, J. Harshan, and E. Viterbo, "Integer-forcing MIMO linear receivers based on lattice reduction," *IEEE Trans. Wireless Commun.*, vol. 12, pp. 4905–4915, Oct. 2013.
- [30] M. M. Amiri and D. Gunduz, "Machine learning at the wireless edge: Distributed stochastic gradient descent over-the-air," to be submitted, 2019.
- [31] A. J. Goldsmith and S.-G. Chua, "Variable-rate variable-power MQAM for fading channels," *IEEE Trans. Commun.*, vol. 45, pp. 1218–1230, Oct. 1997.